

Phase Retrieval for Fresnel Measurements Using a Shearlet Sparsity Constraint

Stefan Loock* Gerlind Plonka†

March 25, 2014

Abstract

We consider the problem of phase retrieval in the Fresnel regime. In recent years, several techniques have been used to solve this problem applying different a-priori assumptions on the two-dimensional object in space such as positivity, finite support and amplitude constraints. In this paper, we propose a new constraint, namely the assumption that the object possesses a sparse representation in a shearlet frame. We show, how a shearlet soft-thresholding procedure can be used for phase reconstruction with Fresnel data. As it turns out, the shearlet sparsity constraint yields reconstruction results that are far superior to the support constraint and similarly well as the support plus positivity constraint.

Key words: phase retrieval, Fresnel transform, compactly supported shearlets, relaxed averaged alternating reflection algorithm

Mathematics Subject Classification: 42C40, 49M20, 65K10, 78A60

1 Introduction

In this paper we consider the phase retrieval problem in the Fresnel regime, where the wave propagation is modelled by the unitary Fresnel propagator $\mathcal{R}_\tau f : \mathbb{R}^2 \rightarrow \mathbb{C}^2$,

$$\mathcal{R}_\tau f(\boldsymbol{\xi}) := \frac{1}{\tau^2} \int_{\mathbb{R}^2} \exp\left(i\pi \frac{\|\mathbf{x} - \boldsymbol{\xi}\|^2}{\tau^2}\right) f(\mathbf{x}) \, d\mathbf{x}.$$

Here, $\mathbf{x} = (x_1, x_2)$ and $\boldsymbol{\xi} = (\xi_1, \xi_2)$ are the coordinates in the spatial resp. the Fresnel domain and $\tau = \sqrt{\lambda d}$ describes experimental parameters, the wavelength λ and the distance d between probe and image plane. This mathematical model is often used in coherent x-ray imaging and can be derived as an approximative solution to the Helmholtz equation, see [11].

Let us assume that $m(\boldsymbol{\xi}) := |\mathcal{R}_\tau f(\boldsymbol{\xi})|$, $\boldsymbol{\xi} \in \Omega \subset \mathbb{R}^2$ are the measured magnitudes of the wanted object $f : \mathbb{R}^2 \rightarrow \mathbb{R}$ in the Fresnel domain where, in practice, Ω is a finite grid. Our goal in phase retrieval is to determine the phase of $\mathcal{R}_\tau f$ from the measurements $m(\boldsymbol{\xi})$. After reconstruction of the phase, the inverse Fresnel transform provides the desired object. Unfortunately, the measurement information $m(\boldsymbol{\xi})$ does not sufficiently constrain the problem, therefore one needs to apply additional a-priori information. A frequently used assumption is that f possesses a compact support in spatial domain that can be well approximated during the reconstruction. However, this constraint may not be satisfied in many applications where one does not consider small isolated objects.

*University of Göttingen, Institute for Numerical and Applied Mathematics, Lotzestr. 16-18, 37083 Göttingen, Germany. Email: s.loock@math.uni-goettingen.de

†University of Göttingen, Institute for Numerical and Applied Mathematics, Lotzestr. 16-18, 37083 Göttingen, Germany. Email: plonka@math.uni-goettingen.de

In this paper we want to explore a new constraint for phase retrieval, namely the assumption that the object to be reconstructed can be sparsely represented in space domain within a so-called shearlet frame. Indeed, shearlets have been shown to provide sparse image representations [14] and are suitable as constraints in image inpainting problems, see [6].

The idea to employ sparsity of images in suitable wavelet bases or frames for regularization of the ill-posed problem of phase retrieval has been used already before. The most acknowledged wavelet approach so far for hologram reconstruction is the so-called Fresnelet construction due to Liebling et al. [16], where a Fresnel transform of a tensor-product spline wavelet basis is used to obtain fresnelets. Further recent approaches involving wavelet methods can be found e.g. in [24, 26, 15, 1]. In [24], a multiresolution approximation of the Fresnel diffraction integral by means of tensor-product Shannon wavelets is proposed. Weng et al. [26] employs the two-dimensional Gabor wavelet transform to the measured hologram and uses only the wavelet coefficients at its peak for phase reconstruction. Langer et al. [15] presents a Fourier-wavelet regularized deconvolution method for solving the inverse problem of phase shift reconstruction, where a shift-invariant redundant discrete wavelet transform with Daubechies filters is used. In [1], an iterative projection method is utilized with the constraint that the measured intensity has a good low-resolution approximation, where the multiscale approach is based on Haar wavelets. However, the tensor-product wavelet transform cannot sparsely char-

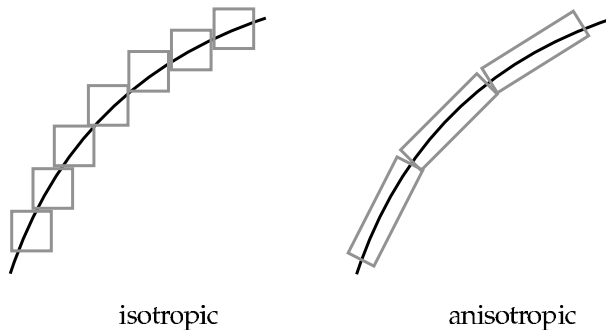


Figure 1: Representation of singularities along curves: isotropic vs. anisotropic scaling.

acterize special two-dimensional structures of images like discontinuities along curves since the wavelet system is not rotationally invariant. However, the Fresnel transform is a unitary transform being translation and rotationally invariant, see [16]. Indeed, we have for $\mathbf{x}_0 \in \mathbb{R}^2$

$$\mathcal{R}_\tau(f(\cdot - \mathbf{x}_0))(\boldsymbol{\xi}) = \mathcal{R}_\tau f(\boldsymbol{\xi} - \mathbf{x}_0),$$

and for a rotation matrix $\mathbf{R}_\theta \in \mathbb{R}^{2 \times 2}$ with angle $\theta \in [0, 2\pi)$ it follows that

$$\mathcal{R}_\tau(f(\mathbf{R}_\theta \cdot))(\boldsymbol{\xi}) = \mathcal{R}_\tau f(\mathbf{R}_\theta \boldsymbol{\xi}).$$

In this paper we examine the applicability of sparsity constraints using shearlets for phase retrieval in the Fresnel regime. Shearlets [6, 12, 17, 14] form a function frame in $L^2(\mathbb{R}^2)$ that is able to represent directional information in images efficiently. Figure 1 illustrates the intrinsic difference between isotropic wavelet functions and anisotropic shearlet functions to detect singularities along curves. In the latter case, much less shearlet functions are necessary to represent the singularities along the smooth curve.

The paper is organized as follows. In Section 2, we summarize the construction of shearlet frames with compact support in space domain due to Lim [17]. In Section 3, we propose a phase reconstruction method based on the relaxed averaged alternating reflection (RAAR) technique introduced by Luke [18, 19] where the new shearlet sparsity constraint is incorporated. This new constraint can be regarded as a smoothing procedure applying a shearlet soft-thresholding. Writing the phase retrieval problem as a feasibility problem for a convex set and a prox-regular set, Luke succeeded to show local convergence of the RAAR algorithm in [19]. Investigating the

properties of the RAAR iteration using the new shearlet sparsity constraint, we observe that the reconstruction problem cannot simply be interpreted as a feasibility problem. However, in the discrete setting we show that the iteration sequence is bounded. Section 4 is devoted to numerical results showing that the new shearlet constraint is far superior to the support constraint only and equally well as using the support plus positivity constraint. For data being corrupted with Poisson noise our reconstruction scheme is further improved by combining the shearlet sparsity constraint with the positivity constraint. In this noisy case the new method considerably outperforms the known conventional methods. The paper is finished by a short conclusion presenting some open problems regarding this approach.

2 The shearlet frame

We briefly summarize the basic idea for the construction of separable shearlets with compact support in spatial domain due to Lim [17] allowing a fast and simple shearlet transform. Let $\phi \in L^2(\mathbb{R})$ be a one-dimensional orthonormal scaling function with compact support, and let $\psi \in L^2(\mathbb{R})$ be an orthonormal compactly supported wavelet function. For example, ϕ can be chosen as a Daubechies scaling function with support $[0, 2n + 1]$ and ψ as the corresponding wavelet function with support $[-n, n + 1]$, see [4]. Other examples are symlets with a sufficient number of vanishing moments [4]. Now, the mother shearlet is defined as

$$\Psi(\mathbf{x}) := \phi(x_1)\psi(x_2).$$

The shearlet frame is generated using translations, scalings and shearings of the mother shearlet, i.e.,

$$\Psi_{j,\ell,\mathbf{k}}(\mathbf{x}) = \left(2^{j\lfloor j/2 \rfloor}\right)^{1/2} \Psi(B^\ell A^j \mathbf{x} - c\mathbf{k}), \quad (2.1)$$

where $\mathbf{k} \in \mathbb{Z}^2$, $c > 0$ is a suitable sampling constant, and where for $j \in \mathbb{N}_0$ and $\ell \in \mathbb{Z}$ with $|\ell| \leq 2^{\lfloor j/2 \rfloor}$,

$$A^j = \begin{pmatrix} 2^{\lfloor j/2 \rfloor} & 0 \\ 0 & 2^j \end{pmatrix}, \quad B^\ell = \begin{pmatrix} 1 & 0 \\ \ell & 1 \end{pmatrix}$$

generate a parabolic scaling resp. a shearing of Ψ . For more details on the shearlet construction we refer to [17]. Figure 2 visualizes, how the supports of shearlet functions change depending on the chosen parameters. Besides $\Psi_{j,\ell,\mathbf{k}}$ we also consider translation, scaling and shearing of the (rotated) mother shearlet $\tilde{\Psi}(\mathbf{x}) := \psi(x_1)\phi(x_2)$ (analogously as in (2.1)) as well as translations of the low-pass function $\Phi(\mathbf{x}) := \phi(x_1)\phi(x_2)$ to construct the complete shearlet frame of $L^2(\mathbb{R}^2)$ of the form

$$\begin{aligned} \{\Phi_{\mathbf{k}} : \mathbf{k} \in \mathbb{Z}^2\} \cup & \{\Psi_{j,\ell,\mathbf{k}} : j \in \mathbb{N}_0, -2^{\lfloor j/2 \rfloor} \leq \ell \leq 2^{\lfloor j/2 \rfloor}, \mathbf{k} \in \mathbb{Z}^2\} \\ \cup & \{\tilde{\Psi}_{j,\ell,\mathbf{k}} : j \in \mathbb{N}_0, -2^{\lfloor j/2 \rfloor} \leq \ell \leq 2^{\lfloor j/2 \rfloor}, \mathbf{k} \in \mathbb{Z}^2\}, \end{aligned}$$

where $\Phi_{\mathbf{k}} := \Phi(\cdot - c\mathbf{k})$. Observe that this shearlet frame (differently from shearlet constructions with band-limited functions) is no longer tight. Tight shearlet frame constructions with compact support can however be given by suitable extension of this shearlet frame, [17].

The shearlet transform maps f to the set of all shearlet coefficients,

$$\mathcal{S}f = \mathbf{c} = ((c_{j,\ell,\mathbf{k}})_{j,\ell,\mathbf{k}}, (\tilde{c}_{j,\ell,\mathbf{k}})_{j,\ell,\mathbf{k}}, (c_{\mathbf{k}})_{\mathbf{k}}),$$

where $c_{j,\ell,\mathbf{k}} := \langle f, \Psi_{j,\ell,\mathbf{k}} \rangle$, $\tilde{c}_{j,\ell,\mathbf{k}} := \langle f, \tilde{\Psi}_{j,\ell,\mathbf{k}} \rangle$, and $c_{\mathbf{k}} := \langle f, \Phi_{\mathbf{k}} \rangle$, and where $\langle \cdot, \cdot \rangle$ denotes the usual L^2 -scalar product.

In [17] it is shown, how the shearlet coefficients can be efficiently computed for $c = 1$ using the underlying multiresolution analysis being similar to separable wavelet transforms.

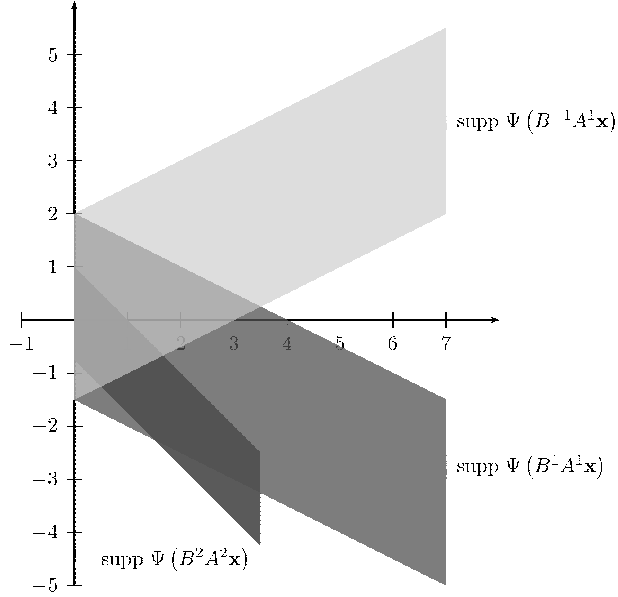


Figure 2: Support of different shearlet functions depending on their scaling and shearing parameters where $\text{supp } \Psi = [0, 7] \times [-3, 4]$.

For simplicity, we regard I_S as a one-dimensional index set for the shearlet coefficients, i.e., $\mathcal{S}f = \mathbf{c} = (c_i)_{i \in I_S}$. In the discrete setting, we assume that f is a discrete image with real-valued entries, i.e., $f : \Omega_s \rightarrow \mathbb{R}$ with $\Omega_s = \{1, \dots, N\} \times \{1, \dots, N\}$ where N is a power of 2. The discrete shearlet transform in [17] on an $N \times N$ image with $N = 2^J$ yields a total number of shearlet coefficients $N_S := \frac{3}{4}(4^J - 1) + \frac{2}{2\sqrt{2}-1}((2\sqrt{2})^J - 1) + 1$, and we have a redundancy ratio $2^{-2J}N_S \leq 2$ for $J \geq 1$. In this case we can regard $\mathbf{c} = (c_i)_{i \in I_S}$ as a vector of length N_S . The inverse transform is based on the application of the pseudo inverse $(\mathcal{S}^* \mathcal{S})^{-1} \mathcal{S}^*$ of the shearlet transform \mathcal{S} , where $\mathcal{S}^* \mathbf{c} = \sum_{i \in I_S} c_i \Psi_i$. It can be efficiently computed using conjugate gradient methods, [17]. Since the shearlets are compactly supported in space, a sparse representation of directional structures in images can be achieved using only a small amount of most significant shearlet coefficients, see [14].

3 Phase reconstruction using the new sparsity constraint

We recall that the Fresnel transform can be written as a convolution of f with the kernel $K_\tau(\mathbf{x}) := \frac{1}{\tau^2} \exp(i\pi(\|\mathbf{x}\|_2/\tau)^2)$ with $\|\mathbf{x}\|_2 = (x_1^2 + x_2^2)^{1/2}$, i.e., we have

$$\mathcal{R}_\tau f(\boldsymbol{\xi}) = (f * K_\tau)(\boldsymbol{\xi})$$

implying

$$\widehat{\mathcal{R}_\tau f}(\boldsymbol{\omega}) = \widehat{f}(\boldsymbol{\omega}) \widehat{K}_\tau(\boldsymbol{\omega}),$$

where the Fourier transform is given by $\widehat{f}(\boldsymbol{\omega}) := \int_{\mathbb{R}^2} f(\mathbf{x}) e^{2\pi i \langle \mathbf{x}, \boldsymbol{\omega} \rangle} d\mathbf{x}$ with $\langle \mathbf{x}, \boldsymbol{\omega} \rangle = x_1 \omega_1 + x_2 \omega_2$. In particular, the Fourier transformed kernel $\widehat{K}_\tau(\boldsymbol{\omega}) := i \exp(-i\pi(\tau \|\boldsymbol{\omega}\|_2)^2)$ obeys similar oscillation properties as K_τ . Hence, in the discrete setting $f \in \mathbb{R}^{N \times N}$, the discrete Fresnel transform and its inverse can be efficiently computed using the two-dimensional Fourier transform on the grid $\Omega_s = \Omega = \{1, \dots, N\} \times \{1, \dots, N\}$. Therefore, we can assume that the discrete Fresnel transform is still unitary.

First we formulate the phase retrieval problem as a feasibility problem using the support

constraint and the positivity constraint. We define

$$\begin{aligned} M &:= \left\{ f \in \mathbb{R}^{N \times N} : |\mathcal{R}_\tau f(\boldsymbol{\xi})| = m(\boldsymbol{\xi}) \forall \boldsymbol{\xi} \in \Omega \right\}, \\ C &:= \left\{ f \in \mathbb{R}^{N \times N} : \text{supp } f \subseteq D \right\}, \\ C_+ &:= \{ f \in C : f(\mathbf{x}) \geq 0 \forall \mathbf{x} \in D \}, \end{aligned} \quad (3.1)$$

i.e., M is the set of matrices satisfying the measurement conditions in the Fresnel domain, and C (resp. C_+) is the set of matrices satisfying the support constraint where D is some subset of Ω_s . Here, for matrices $f = (f(i, j))_{i, j=1}^N$ we denote $\text{supp } f := \{(i, j) \in \Omega_s : f(i, j) \neq 0\}$. Since the (discrete) Fresnel transform is unitary, we observe that all matrices in the set M have the same Frobenius norm,

$$\|f\|_F := \left(\sum_{\mathbf{x} \in \Omega_s} |f(\mathbf{x})|^2 \right)^{1/2} = \left(\sum_{\boldsymbol{\xi} \in \Omega} m(\boldsymbol{\xi})^2 \right)^{1/2} =: B_\Omega. \quad (3.2)$$

Further, the set M is non-convex while C and C_+ are convex sets. Now the *feasibility problem* consists in finding a matrix in the intersection of M and C resp. C_+ , i.e.,

$$\text{find } f \in M \cap C \quad \text{or} \quad \text{find } f \in M \cap C_+. \quad (3.3)$$

The usual approach to solve such a feasibility problem is to apply alternating projection algorithms that have a long standing tradition in the phase retrieval community [9, 25, 8, 7, 2, 18]. We refer to Luke [18] for a comprehensive representation of different projection algorithms as Fienup's Hybrid Input-Output algorithm (HIO) [8], Elser's difference map algorithm [7], and the Hybrid Projection Reflection algorithm (HPR) [2]. In this paper, we want to apply the Relaxed Averaged Alternating Reflection algorithm (RAAR) proposed in [18]. Let P_M and P_C (resp. P_{C_+}) denote the orthogonal projectors on the sets M resp. C (C_+), where

$$P_C f(\mathbf{x}) = \begin{cases} f(\mathbf{x}), & \mathbf{x} \in D, \\ 0 & \text{elsewhere,} \end{cases} \quad P_{C_+} f(\mathbf{x}) = \begin{cases} \max\{f(\mathbf{x}), 0\} & \mathbf{x} \in D, \\ 0 & \text{elsewhere,} \end{cases}$$

and $P_M f(\mathbf{x}) := (\mathcal{R}_\tau^{-1} g)(\mathbf{x})$ with

$$g(\boldsymbol{\xi}) := \begin{cases} \left(m(\boldsymbol{\xi}) \frac{\mathcal{R}_\tau f(\boldsymbol{\xi})}{|\mathcal{R}_\tau f(\boldsymbol{\xi})|} \right) & \text{if } |\mathcal{R}_\tau f(\boldsymbol{\xi})| \neq 0, \\ m(\boldsymbol{\xi}) & \text{if } |\mathcal{R}_\tau f(\boldsymbol{\xi})| = 0, \end{cases} \quad (3.4)$$

for $\boldsymbol{\xi} \in \Omega$.

Further, let $R_M := 2P_M - I$, $R_C := 2P_C - I$ be the corresponding reflectors with respect to M and C , where I denotes the identity operator. Then the RAAR iteration is of the form

$$f_{k+1} = \left[\frac{\beta_k}{2} (R_C R_M + I) + (1 - \beta_k) P_M \right] f_k, \quad (3.5)$$

where the relaxation parameter $\beta_k \in (0, 1]$ can be taken suitably in each iteration step. The initial function f_0 can be chosen as $f_0 = \mathcal{R}_\tau^{-1} m$ such that the initial phase of $\mathcal{R}_\tau f_0$ is zero, or as $f_0 = \mathcal{R}_\tau^{-1} g$ with $g(\boldsymbol{\xi}) = m(\boldsymbol{\xi}) \cdot e^{i\varphi(\boldsymbol{\xi})}$ for all $\boldsymbol{\xi} \in \Omega$ and random phase $\varphi(\boldsymbol{\xi}) \in [0, 2\pi]$.

For $\beta = \beta_k = 1$, the RAAR, HPR, and the difference map (with suitable parameters) are equivalent. For $\beta_k \neq 1$, RAAR is fundamentally different from HPR and cannot be derived as a special difference map, [18]. Compared with other non-relaxed projection algorithms, the advantage of the RAAR approach is its behavior in case of inconsistent feasibility problems, where the intersection $M \cap C$ is empty. It has been shown in [19] that the RAAR algorithm converges for feasibility problems of the type (3.3) for a prox-regular set M and a convex set C , where in the case $M \cap C = \emptyset$, a nearest point minimizing the distance to M and C is found.

In these considerations we can also replace P_C by P_{C_+} thereby replacing the a-priori support constraint by the stronger support plus positivity constraint.

Our goal is now to exchange the support constraint by a new constraint that is based on the sparse representation of the object $f \in \mathbb{R}^{N \times N}$ in a shearlet frame. For that purpose, we introduce the soft-thresholding operator that is defined for a vector $\mathbf{c} = (c_i)_{i \in I_S}$ as

$$(\mathcal{T}_\theta \mathbf{c})_i := \begin{cases} c_i - \theta, & \text{if } c_i > \theta, \\ c_i + \theta, & \text{if } c_i < -\theta, \\ 0, & \text{otherwise} \end{cases} \quad (3.6)$$

with some thresholding parameter $\theta > 0$. Componentwise application of \mathcal{T}_θ to the vector of shearlet coefficients $\mathcal{S}f = \mathbf{c}$ and subsequent inverse transform yields a sparse shearlet approximation $\mathcal{S}^{-1} \mathcal{T}_\theta \mathcal{S}f$ of f . We denote the corresponding shearlet thresholding operator by

$$P_S^\theta f := \mathcal{S}^{-1} \mathcal{T}_\theta \mathcal{S}f. \quad (3.7)$$

The application of the shearlet threshold operator can be equivalently written as $P_S^\theta f = \mathcal{S}^{-1} \mathbf{c}_\theta$, where \mathbf{c}_θ solves the minimization problem

$$\mathbf{c}_\theta = \underset{\mathbf{c}}{\operatorname{argmin}} \left(\theta \|\mathbf{c}\|_1 + \frac{1}{2} \|\mathbf{c} - \mathcal{S}f\|_2^2 \right) \quad (3.8)$$

thereby seeking for a vector \mathbf{c} of shearlet coefficients with a small ℓ_1 -norm that approximates $\mathcal{S}f$. Indeed, componentwise differentiation of (3.8) leads to the condition

$$0 \in \theta \frac{c_i}{|c_i|} + (c_i - (\mathcal{S}f)_i)$$

for the minimizing vector \mathbf{c} , where $\frac{c_i}{|c_i|}$ denotes the set $[-1, 1]$ for $c_i = 0$. Hence, $\mathbf{c}_\theta = \mathcal{T}_\theta \mathcal{S}f$. Using the RAAR algorithm for this new setting, we obtain the iteration

$$f_{k+1} = \left[\frac{\beta_k}{2} (R_S^\theta R_M + I) + (1 - \beta_k) P_M \right] f_k \quad (3.9)$$

with R_M as above and $R_S^\theta := 2P_S^\theta - I$.

In our numerical implementations, the parameters β_k are chosen as in [21], for details we refer to Section 4. Further, it will be reasonable to adapt $\theta = \theta_k$ depending on the iteration k . For a discussion, see Remark 3.3(4) and Section 4.

In the remaining part of this section we want to consider some properties of the RAAR iteration in this setting. First note that neither the projector P_M nor the reflector R_M are contractions since the set M is not convex. Particularly, for matrices f with $\|f\|_F < B_\Omega$ we have $\|f\|_F < \|P_M f\|_F = B_\Omega$. However, we can show that the norm of all f_k , $k \in \mathbb{N}$, in (3.9) is bounded.

Theorem 3.1 *Assume that the considered shearlet frame is tight with frame bound $m > 0$. Then for all f_k , $k \in \mathbb{N}$ (with $f_0 \in M$) obtained by the iteration (3.9) we have*

$$\max\left\{0, B_\Omega - 3\beta_k \frac{\sqrt{N_S} \theta}{m}\right\} \leq \|f_k\|_F \leq B_\Omega + \beta_k \frac{\sqrt{N_S} \theta}{m},$$

where N_S is the number of shearlet coefficients in $\mathcal{S}f$. Further, assuming that $B_\Omega > 0$ and $\beta_k \geq \epsilon > 0$ for all $k \in \mathbb{N}$, there does not exist an $f \in M$ that is a fixed point of the iteration (3.9).

Proof. First we observe from the definition of the soft threshold operator for a tight shearlet frame that

$$\|f - P_S^\theta f\|_F = \frac{1}{m} \|\mathcal{S}f - \mathcal{T}_\theta \mathcal{S}f\|_2 \leq \frac{\sqrt{N_S \theta}}{m}.$$

Further, using (3.2) and $\|P_S^\theta f\|_F < \|f\|_F$ for all $f \in \mathbb{R}^{n \times n} \setminus \{0\}$, we obtain

$$\begin{aligned} \|f_{k+1}\|_F &= \left\| \frac{\beta_k}{2} (R_S^\theta R_M + I) f_k + (1 - \beta_k) P_M f_k \right\|_F \\ &\leq \frac{\beta_k}{2} \|(R_S^\theta R_M + I) f_k\|_F + (1 - \beta_k) B_\Omega \\ &\leq \frac{\beta_k}{2} (\|R_S^\theta (R_M + I) f_k\|_F + \|(I - R_S^\theta) f_k\|_F) + (1 - \beta_k) B_\Omega \\ &\leq \frac{\beta_k}{2} \left(2B_\Omega + 2 \frac{\sqrt{N_S \theta}}{m} \right) + (1 - \beta_k) B_\Omega \\ &= B_\Omega + \beta_k \frac{\sqrt{N_S \theta}}{m}. \end{aligned}$$

In the last inequality we have used that the reflector R_S^θ also satisfies $\|R_S^\theta f\|_F \leq \|f\|_F$. Similarly,

$$\begin{aligned} \|f_{k+1}\|_F &= \left\| \frac{\beta_k}{2} (R_S^\theta R_M + I) f_k + (1 - \beta_k) P_M f_k \right\|_F \\ &= \left\| \frac{\beta_k}{2} ((2P_S^\theta - I)(2P_M - I) + I) f_k + (1 - \beta_k) P_M f_k \right\|_F \\ &= \|P_M f_k + 2\beta_k (P_S^\theta P_M - P_M) f_k + \beta_k (I - P_S^\theta) f_k\|_F \\ &\geq \|(I + 2\beta_k (P_S^\theta - I) P_M) f_k\|_F - \beta_k \|(I - P_S^\theta) f_k\|_F \\ &\geq \|P_M f_k\|_F - 2\beta_k \frac{\sqrt{N_S \theta}}{m} - \beta_k \frac{\sqrt{N_S \theta}}{m} = B_\Omega - 3\beta_k \frac{\sqrt{N_S \theta}}{m}. \end{aligned}$$

Moreover, we have

$$\begin{aligned} f_{k+1} - f_k &= \frac{\beta_k}{2} (R_S^\theta (2P_M - I) f_k - f_k) + (1 - \beta_k) (P_M - I) f_k \\ &= \frac{\beta_k}{2} (R_S^\theta P_M - I) f_k + \left(\frac{\beta_k}{2} R_S^\theta + (1 - \beta_k) I \right) (P_M - I) f_k. \end{aligned}$$

Hence, for $f_k \in M$ it follows from $f_k = P_M f_k$ that

$$f_{k+1} - f_k = \frac{\beta_k}{2} (R_S^\theta P_M - I) f_k = \beta_k (P_S^\theta - I) f_k \neq 0$$

since $B_\Omega > 0$, i.e., there exists no fixed point $f \in M$ of this iteration. ■

Theorem 3.1 implies that the sequence $(f_k)_{k \in \mathbb{N}}$ possesses at least one accumulation point. Attempting to write the reconstruction problem with the shearlet constraint again as a feasibility problem, the observations in Theorem 3.1 may suggest to define the set of matrices satisfying the shearlet sparsity constraint by

$$S := \left\{ f \in \mathbb{R}^{N \times N} : \mathcal{S}f = \mathcal{T}_\theta \mathcal{S}h, h \in \mathbb{R}^{N \times N}, \|\mathcal{S}h\|_2 \leq \tilde{B}_\Omega \right\}, \quad (3.10)$$

where we may choose $\tilde{B}_\Omega \geq mB_\Omega + \sqrt{N_S \theta}$ with m being the frame bound of the shearlet frame. For a tight frame we can replace the condition $\|\mathcal{S}h\|_2 \leq \tilde{B}_\Omega$ in (3.10) by $\|h\|_F \leq \tilde{B}_\Omega/m$.

Obviously P_S^θ is not a projector on S (for $\tilde{B}_\Omega > 0$) since it is not idempotent and retains only the most significant shearlet coefficients of f . But P_S^θ is a so-called proximal mapping,

see [23], Definition 1.22, thereby generalizing the concept of iterated projection algorithms, see [5]. More precisely, we have $\mathcal{T}_\theta \mathcal{S}f = \mathbf{c}_\theta = \text{prox}_{\theta|\cdot|}(\mathcal{S}f)$, see e.g. [5], Definition 2.1.

However, the choice of the bound $\tilde{B}_\Omega > 0$ and hence the size of the set S does not effect the result of the iteration algorithm in (3.9). This is particularly according to the fact that we do not employ a projection onto S but the proximal mapping P_S^θ which is a contractive mapping. Since the ℓ_1 -norm is lower semi-continuous, we know that the proximal mapping $\text{prox}_{\theta|\cdot|}$ is firmly nonexpansive. Especially, we have $\|P_S^\theta f\|_F < \|f\|_F$ for $\|f\|_F > 0$ such that for $f \in M$ the matrix $P_S^\theta f$ is not longer contained in M . Therefore only a “relaxed” iterative projection algorithm is suitable for incorporating the shearlet sparsity condition. Unfortunately we even find the following result indicating that we cannot simply apply the results on local convergence of the RAAR algorithm in our setting.

Lemma 3.2 *The set S in (3.10) is not convex.*

Proof. Let h_1, h_2 be two matrices with $\mathcal{S}h_1 = (\tilde{B}_\Omega, 0, \dots, 0)^T$ and $\mathcal{S}h_2 = (\sqrt{\tilde{B}_\Omega^2 - (\theta + \epsilon)^2}, (\theta + \epsilon), 0, \dots, 0)^T$ with $\epsilon > 0$ determining two matrices f_1 and f_2 in the set S by

$$\mathcal{S}f_1 = \mathcal{T}_\theta \mathcal{S}h_1 = (\tilde{B}_\Omega - \theta, 0, \dots, 0)^T, \quad \mathcal{S}f_2 = \mathcal{T}_\theta \mathcal{S}h_2 = (\sqrt{\tilde{B}_\Omega^2 - (\theta + \epsilon)^2} - \theta, \epsilon, 0, \dots, 0)^T.$$

Consider now the matrix $\frac{1}{2}(f_1 + f_2)$ with

$$\frac{1}{2}(\mathcal{S}f_1 + \mathcal{S}f_2) = \left(\frac{1}{2}(\tilde{B}_\Omega - \theta) + \frac{1}{2}(\sqrt{\tilde{B}_\Omega^2 - (\theta + \epsilon)^2} - \theta), \frac{\epsilon}{2}, 0, \dots, 0\right).$$

Then $\mathcal{S}h = \left(\frac{1}{2}\left(\tilde{B}_\Omega + \sqrt{\tilde{B}_\Omega^2 - (\theta + \epsilon)^2}\right), \frac{\epsilon}{2} + \theta, 0, \dots, 0\right)$ is the vector with minimal norm satisfying $\frac{1}{2}(\mathcal{S}f_1 + \mathcal{S}f_2) = \mathcal{T}_\theta \mathcal{S}h$. But for sufficiently small ϵ we obtain

$$\left(\frac{1}{2}\left(\tilde{B}_\Omega + \sqrt{\tilde{B}_\Omega^2 - (\theta + \epsilon)^2}\right)\right)^2 + \left(\frac{\epsilon}{2} + \theta\right)^2 > \tilde{B}_\Omega^2.$$

since for $\epsilon \rightarrow 0$ we easily observe that

$$\frac{1}{4}\left(\tilde{B}_\Omega + \sqrt{\tilde{B}_\Omega^2 - \theta^2}\right)^2 + \theta^2 > \tilde{B}_\Omega^2,$$

where we can assume by construction that $\tilde{B}_\Omega > \sqrt{\frac{3}{2}}\theta$. Hence $\frac{1}{2}(f_1 + f_2) \notin S$. ■

Remarks 3.3

(1) In [19, 20], Luke succeeded to show that the RAAR algorithm for solving a feasibility problem of the form

$$\text{find } f \in A \cap B$$

possesses local linear convergence properties, if one set A is prox-regular and the other set is convex. In the feasibility problems of the type (3.3) considered here, the set C (resp. C_+) is convex. Unfortunately, M is neither convex nor prox-regular. But a regularization of M of the form

$$M_\epsilon := \{f \in \mathbb{R}^{N \times N} : d(|\mathcal{R}_\tau f|, m) < \epsilon\}$$

with $\epsilon > 0$ can be shown to be prox-regular, where the distance function d can be e.g. the Euclidean norm, or more generally a Bregman distance, see [20], Section 3. A “fattening” of the original set M to obtain M_ϵ is also meaningful in practice if the data m are noisy, and the distance function can be chosen according to the noise distribution. However, since the incorporation of the shearlet constraint cannot be nicely written as a feasibility problem, we do

not see any possibility to directly apply the results on local convergence of the RAAR algorithm given in [19, 20] in our case. Despite this fact, a suitable fattening of the set M may also lead to local convergence of the iteration sequence (3.9) in our setting.

(2) While the set S in (3.10) is not convex, one can simply obtain a convex set by changing the norms and taking e.g.

$$\tilde{S} := \left\{ f \in \mathbb{R}^{N \times N} : \mathcal{S}f = \mathcal{T}_\theta \mathcal{S}h, h \in \mathbb{R}^{N \times N}, \|\mathcal{S}h\|_\infty \leq \tilde{B}_\Omega \right\},$$

where $\|\cdot\|_\infty$ denotes the usual maximum norm. Indeed from the definition of \mathcal{T}_θ it follows that \tilde{S} is the set of all matrices f whose shearlet transform is bounded by $\|\mathcal{S}f\|_\infty \leq \tilde{B}_\Omega - \theta$.

(3) Instead of applying the soft threshold operator \mathcal{T}_θ as proposed in (3.6), we may also employ another threshold function. Particularly for the hard threshold

$$(\mathcal{T}_\theta^H \mathbf{c})_i := \begin{cases} c_i & \text{if } |c_i| > \theta, \\ 0 & \text{if } |c_i| \leq \theta, \end{cases}$$

we can similarly define a shearlet threshold operator $P_S^{H,\theta} := \mathcal{S}^{-1} \mathcal{T}_\theta^H \mathcal{S}f$. This operator is idempotent, and hence a projector. However, any resulting set S that may be defined similarly as in (3.10) will be not convex since it contains holes in the shearlet coefficient domain where small coefficients are projected to zero. Therefore, the available theoretical results from convex analysis do not apply also in this case. Further, our numerical experiments show that the choice of the soft threshold operator yields better reconstruction results.

(4) As shown in Theorem 3.1, the sequence (f_k) in (3.9) cannot have a fixed point in M for $\beta_k \geq \epsilon > 0$ and $\theta > 0$. This observation suggests to employ a step-dependent thresholding parameter θ_k that decreases for $k \rightarrow \infty$. A large θ_k implies a sparser shearlet representation yielding stronger data denoising but may also introduce unwanted blurring. The smaller the θ_k , the ‘‘closer’’ the obtained f_k will be to the set M .

(5) In our numerical considerations we will apply a slightly different definition of the operator P_M than given in (3.4) that has been shown to be considerably more stable, see [22]. It is based on a smooth perturbation of the modulus function $|\mathcal{R}_\tau f_k(\boldsymbol{\xi})|$ and aims to minimize the error

$$E_\epsilon(f) := \sum_{\boldsymbol{\xi} \in \Omega} \left| \frac{|\mathcal{R}_\tau f(\boldsymbol{\xi})|^2}{(|\mathcal{R}_\tau f(\boldsymbol{\xi})|^2 + \epsilon)^{1/2}} - m(\boldsymbol{\xi}) \right|^2,$$

where $0 < \epsilon \ll 1$. Following the considerations in [22], Section 5.2, and taking into account that the Fresnel transform is an isometric map, we arrive at the representation $P_M f(\mathbf{x}) := (\mathcal{R}_\tau^{-1} g)(\mathbf{x})$, where instead of (3.4) the formula

$$g_\epsilon(\boldsymbol{\xi}) := (\mathcal{R}_\tau f)(\boldsymbol{\xi}) \left[1 - \left(\frac{|\mathcal{R}_\tau f(\boldsymbol{\xi})|^2 + 2\epsilon}{(|\mathcal{R}_\tau f(\boldsymbol{\xi})|^2 + \epsilon)^{3/2}} \right) \left(\frac{|\mathcal{R}_\tau f(\boldsymbol{\xi})|^2}{(|\mathcal{R}_\tau f(\boldsymbol{\xi})|^2 + \epsilon)} - m(\boldsymbol{\xi}) \right) \right] \quad (3.11)$$

is used. Under suitable assumptions, it follows $\lim_{\epsilon \rightarrow 0} g_\epsilon(\boldsymbol{\xi}) = g(\boldsymbol{\xi})$.

4 Numerical Examples

We apply the new iteration scheme incorporating the shearlet sparsity constraint

$$f_{k+1} = \left[\frac{\beta_k}{2} \left(R_S^{\theta_k} R_M + I \right) + (1 - \beta_k) P_M \right] f_k \quad (4.1)$$

to object reconstruction. We use an implementation of the RAAR algorithm from the *Prox-Toolbox* [21] to recover the lost phase and to reconstruct $f(\mathbf{x})$ from its propagated version

$\mathcal{R}_\tau f(\xi)$. This toolbox is available from <http://num.math.uni-goettingen.de/r.luke/publications/publications.html>. The shearlet transform is computed using the ShearLab toolbox available from <http://www.shearlet.org>. For the Fresnel transform we use the implementation provided by [16] from <http://sybil.ece.ucsb.edu/pages/fresnelab/fresnelab.html>.

In all experiments, the parameter β_k is chosen in dependence of the iteration step with $\beta_0 = 0.95$, $\beta_{\text{switch}} = 20$, and $\beta_{\text{max}} = 0.55$ by

$$\beta_k = \exp((-k/20)^3) * 0.95 + (1 - \exp((-k/20)^3)) * 0.55$$

as proposed in the ProxToolbox [21]. For the regularization parameter ϵ in (3.11) we take $\epsilon = 10^{-10}$. Further, the choice of the soft thresholding parameter θ_k has strong influence on the numerical results, see Remark 3.3(4). Our experiments show promising results for decreasing θ_k in dependence of the iteration number k in the noiseless case where we have found $\theta_0 = 0.5$ and $\theta_k = \theta_0/k$ to be a suitable parameter choice. In the case of Poisson distributed data, $\theta_k \equiv \theta_0$ is taken to be constant.

For the noiseless case we obtain the following numerical scheme.

Algorithm 4.1

Input: data $f_1 = \mathcal{R}_\tau^{-1}(m)$, parameters $\theta_0, \beta_0, \beta_{\text{max}}, \beta_{\text{switch}}$, number of iterations N

Output: f_N

Iteration:

for $k = 1, \dots, N$

$$\theta_k \leftarrow \theta_0/k$$

$$\beta_k \leftarrow \exp\left([-k/\beta_{\text{switch}}]^3\right) * \beta_0 + \left(1 - \exp\left([-k/\beta_{\text{switch}}]^3\right)\right) * \beta_{\text{max}}$$

$$u_k \leftarrow 2P_M f_k - f_k$$

$$f_{k+1} \leftarrow \frac{\beta_k}{2} \left(2P_S^{\theta_k} u_k - u_k + f_k\right) + (1 - \beta_k) P_M f_k$$

end

The complexity of the algorithm is governed by the computation of the mappings $P_M f_k$ and $P_S^{\theta_k} u_k$ at each iteration step. Using the fast Fourier transform for an $N \times N$ image, the projection $P_M f_k$ (containing a discrete Fresnel transform, the componentwise multiplication in (3.4) and an inverse discrete Fresnel transform) requires $\mathcal{O}(N^2 \log N)$ operations. The fast discrete shearlet transform that is employed to compute $P_S^{\theta_k} u_k$ can be implemented with only $\mathcal{O}(N^2)$ operations, see [17]. Therefore this algorithm is only slightly more expensive than the corresponding iteration (3.5) involving the support and positivity constraint.

In our numerical experiments, we also want to employ a stronger version of our proposed shearlet sparsity constraint. Besides forcing a sparse expansion of f in a shearlet frame, we assume that f is real and positive. For this purpose we replace the operator P_S^θ in (3.7) by

$$P_{S_+}^\theta = [\mathcal{S}^{-1} T_\theta \mathcal{S} f]_+$$

with $[\cdot]_+ = \max\{\text{Re}(\cdot), 0\}$. Note that the operation $[\cdot]_+$ itself is a projection onto a convex set. Now we determine the reflector $R_{S_+}^\theta := 2P_{S_+}^\theta - I$ and replace $R_S^{\theta_k}$ by $R_{S_+}^{\theta_k}$ in the iteration scheme (4.1) resp. in Algorithm 4.1.

First, we study two examples of phase retrieval in the noiseless case and compare the reconstruction results using the support constraint and the shearlet sparsity constraint where the support set D is a given rectangular box around the object f . Further, we consider the reconstruction performance when using the positivity constraint additionally. The parameters for the Fresnel transform are $\lambda = 1\text{\AA}$, $d = 100\text{mm}$, the pixel size is $\text{dx} = 10^{-7}\text{m}$ and the images are 256×256 pixels in size. These parameters correspond to coherent imaging experiments using hard x-rays, see [13]. In all cases, we apply Algorithm 4.1 (or its variant) with $N = 250$ iterations.

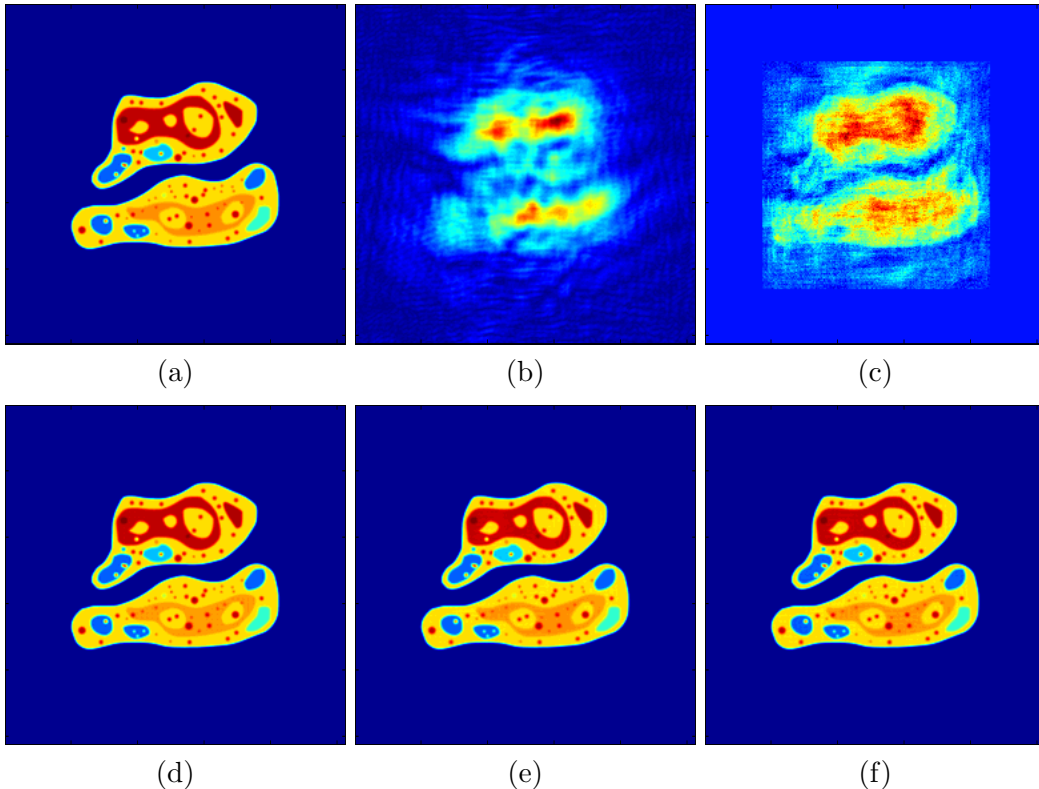


Figure 3: (a) Original image, (b) measurements, (c) reconstruction using the support constraint, (d) support and positivity constraint, (e) shearlet sparsity constraint, (f) shearlet sparsity with positivity constraint.

In Figure 3(a) we take a synthetic image of a cell¹ from [10]. Figure 3(b) represents the magnitudes of Fresnel transform measurements. Figure 3(c) shows, that even without noise, inexact knowledge of the support is not sufficient to recover the image and to eliminate artifacts. Only with further assumptions like positivity a suitable reconstruction is obtained, see Figure 3(d).

On the other hand, using the shearlet sparsity constraint in Figure 3(e), we obtain a solution that is very close to the original image in Figure 3(a) without any assumptions on support or positivity of the function. Finally, Figure 3(f) provides the result when the shearlet sparsity is combined with the positivity constraint. Figure 4 quantitatively compares the difference to the original image $\|f - f_k\|_F$ using the Frobenius norm for the first 100 iterations.

In a second numerical example using a real image taken from [3], Figure 5 shows the original data (a)², the measurements (b) obtained by applying the Fresnel transform with parameters as above, and the reconstruction results using the support constraint (c), the support constraint with additional positivity constraint (d), the proposed shearlet sparsity constraint (e) as well as the shearlet sparsity plus positivity (e).

Also in this case, the shearlet constraint achieves higher resolution and less artifacts than

¹Reprinted Figure 3(a) with permission from K. Giewekemeyer, S.P. Krüger, S. Kalbfleisch, M. Bartels, C. Beta, and T. Salditt, X-ray propagation microscopy of biological cells using waveguides as a quasipoint source, *Phys. Rev. A*, 83:023804 (2011). Copyright (2014) by the American Physical Society.

²Reprinted Figure 3.2 with permission from K. Bredies and D. Lorenz, *Mathematische Bildverarbeitung, Einführung in Grundlagen und moderne Theorie*, Vieweg+Teubner, 2011, p. 59, chapter “3 Grundlegende Werkzeuge”; with kind permission from Springer Science+Business Media B.V.

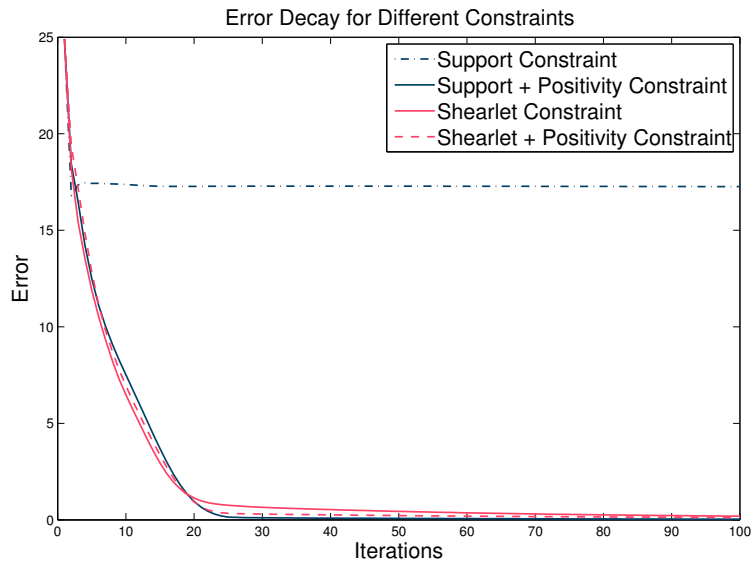


Figure 4: Error decay for all constraints measured in the Frobenius norm.

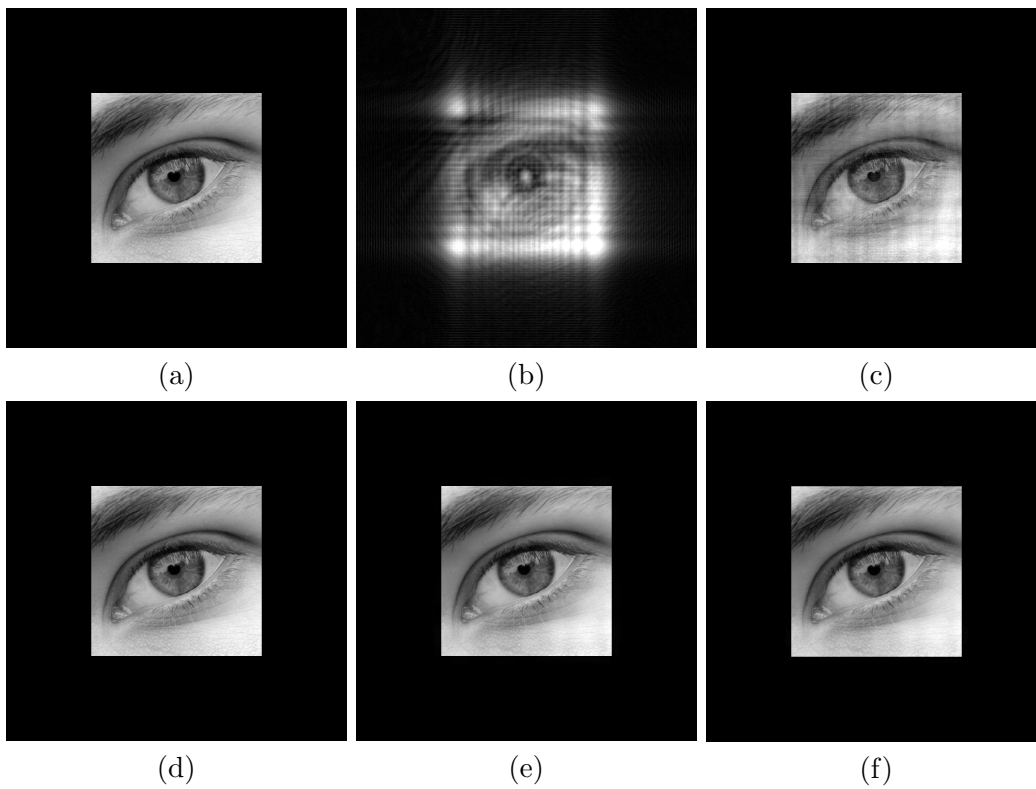


Figure 5: (a) Original image, (b) measurements, (c) reconstruction using the support constraint, (d) support and positivity constraint, (e) shearlet sparsity constraint, (f) shearlet sparsity with positivity constraint.

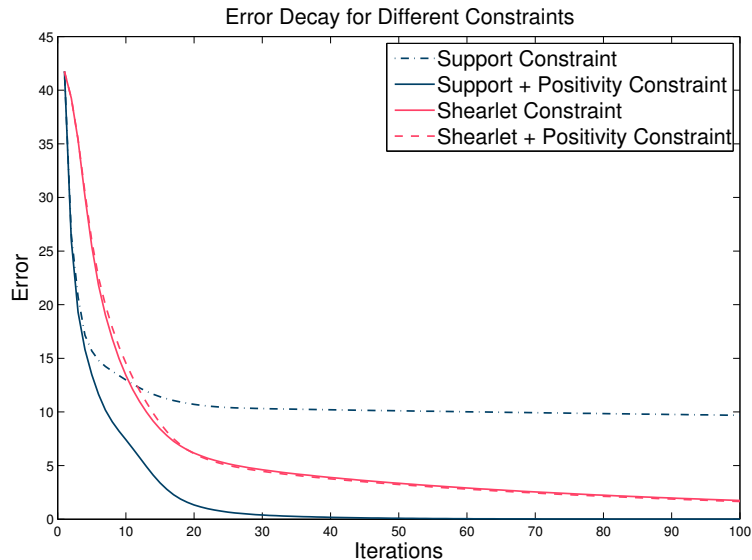


Figure 6: Error decay for all constraints measured in the Frobenius norm.

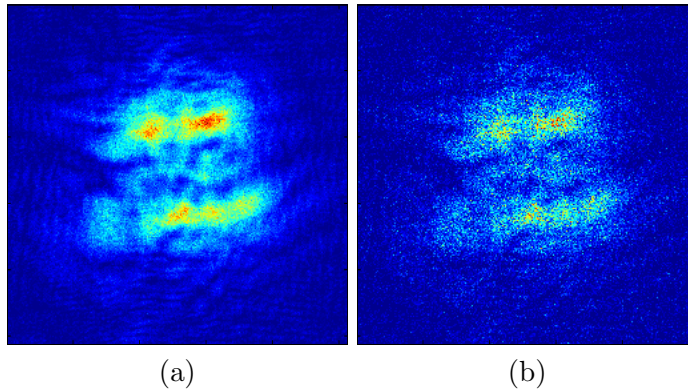


Figure 7: (a) Measurements with Poisson distributed data with $t = 10^6$ counted photons, (b) Measurements with Poisson distributed data with $t = 10^5$ counted photons

the support constraint, as it can be seen in Figure 6, where errors are compared in the Frobenius norm for the first 100 iterations. Additionally, it performs comparably well to the case with support and positivity constraint without forcing the object to be positive and without any knowledge of the support that is often not known in application. The combination of shearlet sparsity and positivity does not gain much in this case.

In real applications we have to apply the reconstruction scheme to Poisson distributed data. Poisson noise is the basic form of uncertainty associated with the measurement of light. The scene irradiance is measured by counting the number of discrete photons incident on the sensor over a given time interval. The detection of the individual photons is a classical Poisson process. Here, the exposure time is proportional to the expected total number t of counted photons.

In a third example we consider data that is Poisson distributed. Observe that in every iteration step f_k is pushed to satisfy the given (noisy) measurement constraints. Therefore the denoising behavior of the shearlet threshold procedure is highly desirable and we fix $\theta_k \equiv 2.5$ for every k in this case. Note that despite assuming f to be real and positive, we do not need any information on the support of f .

We consider the Poisson distributed data in Figure 7 with $t = 10^6$ counted photons (left)

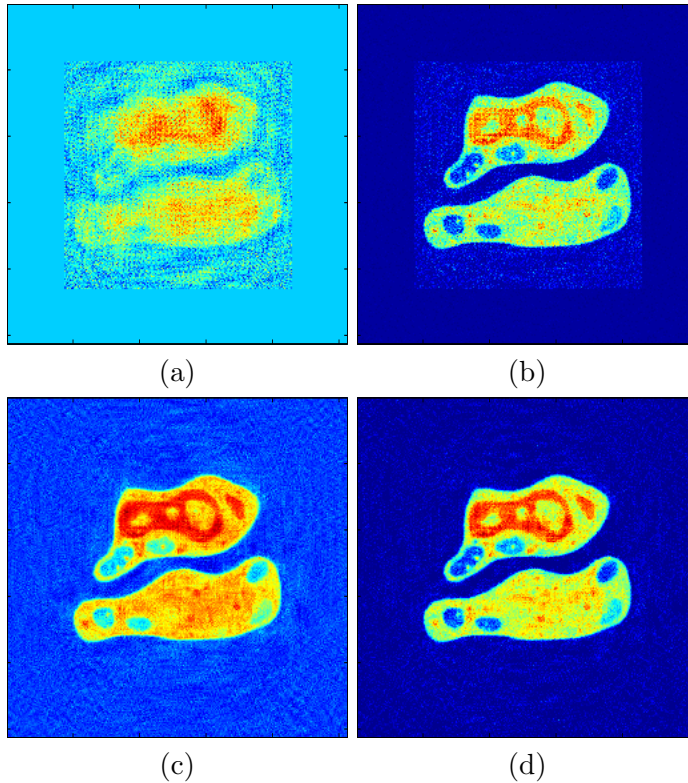


Figure 8: (a) Reconstruction from measurements with $t = 10^6$ counted photons using support constraint, (b) support and positivity constraint, (c) shearlet sparsity constraint, (d) shearlet sparsity constraint with positivity.

and with $t = 10^5$ counted photons (right). The reconstruction results are presented in Figures 8 and 9. Again, we have compared the reconstruction using (a) the support constraint only; (b) the support plus positivity constraint; (c) the new shearlet sparsity constraint; and (d) the shearlet sparsity plus positivity constraint. For $t = 10^6$ counted photons, our algorithm using the shearlet sparsity constraint yields reconstruction results that are comparable to the results using the support plus positivity constraint. However, incorporating the additional assumption that the object is real and positive outperforms the traditional approach drastically, see Figure 8. For $t = 10^5$ the new combination of shearlet sparsity and positivity still yields an acceptable reconstruction result while all other methods completely fail, see Figure 9.

5 Conclusion

The proposed method incorporating the shearlet sparsity constraint shows highly promising results that motivate further research in this direction. Since shearlets provide (almost) optimally sparse representations of two-dimensional functions which are smooth away from \mathcal{C}^2 -singularities [14], this approach strongly improves the reconstruction results in comparison with using only the support constraint and is comparable to support and additional positivity constraints.

The use of an adaptive shearlet threshold parameter θ_k gives the possibility to tune the smoothing behavior during the reconstruction process. We consider problem-dependent parameter choice rules as an open topic for future research. If the data is Poisson distributed, the combination of the shearlet sparsity constraint with the positivity constraint turns out to improve the performance drastically.

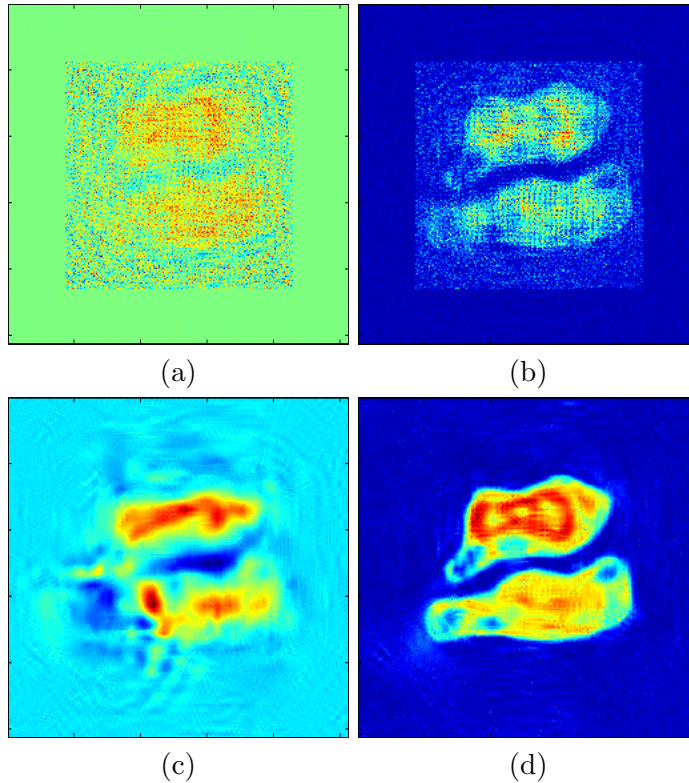


Figure 9: (a) Reconstruction from measurements with $t = 10^5$ counted photons using support constraint, (b) support and positivity constraint, (c) shearlet sparsity constraint (d) shearlet sparsity constraint with positivity.

Future research will also cover the adaption of the approach to phase reconstruction for far field measurements as well as the application to experimental data. Further, it is possible to exploit the new shearlet constraint together with regularization techniques using Gauss-Newton methods.

Acknowledgement

We would like to thank the reviewers for their helpful comments in order to improve the representation of the results in this paper. We gratefully acknowledge the funding of this work by the German Research Foundation (DFG) in the framework of SFB 755 ‘Nanoscale Photonic Imaging’.

References

- [1] L. Baghaei and A. Rad and B. Dai and P. Pianetta and R.F.W. Pease and J. Miao, Iterative phase recovery using wavelet domain constraints, *J. Vac. Sci. Technol. B* **27**, 3192–3195 (2009).
- [2] H. H. Bauschke, P. L. Combettes, and D. R. Luke, Hybrid projection-reflection method for phase retrieval, *J. Opt. Soc. Amer. A*, **20**, 1025–1034 (2003).
- [3] K. Bredies and D. Lorenz, *Mathematische Bildverarbeitung: Einführung in Grundlagen und moderne Theorie*, Vieweg+Teubner, Wiesbaden (2011).

- [4] I. Daubechies, Ten Lectures on Wavelets, Society for Industrial and Applied Mathematics, Philadelphia (1992).
- [5] C. Chaux, P. L. Combettes, J.-C. Pesquet, and V. R. Wajs, A variational formulation for frame-based inverse problems, *Inverse Problems* **23**(4), 1495–1518 (2007).
- [6] G. Easley, W.-Q Lim and D. Labate, Sparse directional image representations using the discrete shearlet transform, *Appl. Comput. Harmon. Anal.* **25**, 25–46 (2008).
- [7] V. Elser, Phase retrieval by iterated projections, *J. Opt. Soc. Amer. A*, **20**, 40–55 (2003).
- [8] J. R. Fienup, Phase retrieval algorithms: A comparison, *Appl. Opt.* **21**, 2758–2769 (1982).
- [9] R. W. Gerchberg and W. O. Saxton, A practical algorithm for the determination of phase from image and diffraction phase pictures, *Optik* **35**, 237–246 (1972).
- [10] K. Giewekemeyer, S. P. Krüger, S. Kalbfleisch, M. Bartels, C. Beta, and T. Salditt, X-ray propagation microscopy of biological cells using waveguides as a quasipoint source, *Phys. Rev. A*, **83**:023804 (2011).
- [11] J. W. Goodman, Introduction to Fourier Optics, McGraw-Hill Series in Electrical and Computer Engineering (2005).
- [12] K. Guo and D. Labate, Representation of Fourier integral operators using shearlets, *J. Fourier Anal. Appl.* **14**, 327–371(45) (2008).
- [13] M. Krenkel, M. Bartels, T. Salditt, Transport of intensity phase reconstruction to solve the twin image problem in holographic x-ray imaging *Opt. Express* **21** (2), 2220–2235 (2013).
- [14] G. Kutyniok and W.-Q Lim, Compactly supported shearlets are optimally sparse. *J. Approx. Theory* **163**, 1564–1589 (2011).
- [15] M. Langer and P. Cloetens and and F. Peyrin, Fourier-wavelet regularization of phase retrieval in x-ray in-line phase tomography, *J. Opt. Soc. Am. A* **26**(8), 1876–1881 (2009).
- [16] M. Lieblich, T. Blu, and M. Unser, Fresnelets: new multiresolution wavelet bases for digital holography, *IEEE Trans. Image Process.* **12**, 29–43 (2003).
- [17] W.-Q. Lim, The discrete shearlet transform: A new directional transform and compactly supported shearlet frames, *IEEE Trans. Image Process.* **19**(2), 1166–1180 (2010).
- [18] R. Luke, Relaxed averaged alternating reflections for diffraction imaging, *Inverse Problems* **21**, 37–50 (2005).
- [19] R. Luke, Finding best approximation pairs relative to a convex and a prox-regular set in a Hilbert space , *SIAM J. Opt.* **19**(2), 714–739 (2008).
- [20] R. Luke, Local linear convergence of approximate projections onto regularized sets, *Non-linear Analysis* **75**, 1531–1546 (2012).
- [21] R. Luke, ProxToolbox, A toolbox of algorithms and projection operators for implementing fixed point iterations based on the Prox operator (2012), <http://num.math.uni-goettingen.de/~r.luke/publications/publications.html>.
- [22] R. Luke, J.V. Burke and R.G. Lyon, Optical wavefront reconstruction: theory and numerical methods, *SIAM Review* **44**(2), 169–224 (2002).
- [23] R.T. Rockafellar and R. J.-B. Wets, Variational Analysis, Springer, 1998.
- [24] A. Souvorov and T. Ishikawa and A. Kuyumchyan, Multiresolution phase retrieval in the Fresnel region by wavelet transform, *J. Opt. Soc. Am. A* **23**(2), 279–287 (2006).
- [25] J. von Neumann, Functional Operators: Vol. II, Princeton University Press (1950).
- [26] J. Weng and J. Zhong and C. Hu, Phase reconstruction of digital holography with the peak of the two-dimensional Gabor wavelet transform, *Appl. Opt.* **48**(18), 3308–3316 (2009).